al Kimiya: Jurnal Ilmu Kimia dan Terapan
p-ISSN: 2407-1897, e-ISSN: 2407-1927
Vol. 10, No. 2 (87-97), December 2023/Jumada al-Akhirah 1445

EFFECT OF PREPARATION ACETONE ON FISH BONES SYNTHESIZED THROUGH SINTERING METHOD TO IMPROVE HYDROXYAPATITE CHARACTERISTICS

RATNA KUSUMAWARDANI[1,2], ATIEK ROSTIKA NOVIYANTI[1*], MUKHAMAD NURHADI[2], AND AKRAJAS ALI UMAR[3]

[1]Department of Chemistry, Faculty of Mathematics and Natural Sciences, Universitas Padjadjaran, Bandung - Sumedang km. 21 Jatinangor Street, Sumedang, Jawa Barat, 45363, Indonesia

[2]Department of Chemistry Education, Faculty of Teacher and Educational Science, Universitas Mulawarman, Kampus Gunung Kelua, Samarinda, 75119, Kalimantan Timur, Indonesia

[3]Institute of Microengineering and Nanoelectronics, Universiti Kebangsaan Malaysia, Bangi, Selangor 43600, Malaysia

*Corresponding Author email: atiek.noviyanti@unpad.ac.id

Informasi Artikel

Received: Sep 05, 2023
Revised: Nov 21, 2023
Accepted: Dec 15, 2023
Published: Dec 31, 2023

DOI:
10.15575/ak.v10i2.29422

Abstrak

In the development of advanced materials and various technological applications, the preparation and sintering processes have become two important factors in determining material characteristics. This research focuses on two main aspects, namely the effect of fish bone preparation by soaking in acetone and the surface area of the material in the sintering process as part of the process of developing better materials. This research aims to determine the effect of soaking fish bone powder with acetone and the effect of the surface area of sintered fish bones to produce hydroxyapatite (HA). The immersion process with acetone is included in the sample preparation stage, while the sintering process is included in the material synthesis stage. These two things can affect the characteristics of the HA produced after analysis from the X-ray diffraction test. The HA structure obtained from all samples is hexagonal with cell parameter values a = b ≠ c and space group P 63 / m, where all samples have a value range of a = b = 9,42 Å and c = 6,88 Å. HA crystallinity was identified through the XRD peak at 2θ = 25,8 (002); 31,7 (211); 32,1 (112); 32,8 (300); 34,0 (202); 39,7 (310); 46,6 (222); 49,4 (213); 50,4 (321). The PAF-900 and CAF-900 samples are similar to HA in JCPDS 01-089-4405 whose compound formula is Ca5(PO4)3(OH) while the PWAF-900 sample is similar to HA in JCPDS 01-075-3727 whose compound formula is $Ca_5(PO_4)_3(CO_3)_{0.01}(OH)_{1.3}$. The percentage of crystallinity of PAF-900, CAF-900, and PWAF-900 respectively was 84,767; 73,506; and 71,962% with HA grain sizes of 0,8964; 0,6808, and 0,7398 nm. The HA density of PAF-900 and CAF-900 samples is 3,149 g/cm^3 while PWAF-900 is 3,146 g/cm^3. Based on this description, it can be concluded that the soaking preparation stage with acetone produces HA with the chemical formula $Ca_5(PO_4)_3OH$ with a higher percentage of crystallization and is denser compared to HA obtained without going through the soaking preparation stage with acetone. The sintering stage also plays an important role in increasing the crystallization percentage. The surface area of the material being sintered also influences the percentage of crystallization and the grain size of the resulting HA. Sintered fish bone powder produces a greater percentage of crystallization and grain size than fish bone chunks.

Keywords:
fish bones; preparation; acetone immersion; sintering; hydroxyapatite.

INTRODUCTION

Hydroxyapatite (HA) is a calcium phosphate compound, with the general formula $M_{10}(RO_4)X_2$ where R is usually the element phosphorus, M is one of the metal elements that is usually the element calcium, and X is usually a hydroxide or element halogens, which act as the main inorganic constituents in bones and teeth and represent biomineralization and bioinspiration [1-3]. During the bone mineral biomineralization process, amorphous calcium phosphate (ACP) is converted into apatite crystals using octacalcium phosphate (OCP) and brushite (DCPD) as precursors meanwhile, resulting in the formation of hybrid nanostructured collagen/apatite composites. HA as the main inorganic component of bone constituents amounts to about 60-70% of the total bone mass

while the organic phase consisting mostly of type I collagen amounts to about 30% of the weight of bone mass, while the rest consists of 5-8% water [4-7]. Therefore, HA is reported as a potential therapeutic ingredient and is applied in spinal fusion surgery, bone defect treatment, bone-related surgery, bone mass augmentation [8], bone replacement material [9], tissue engineering [10], and as a drug carrier [11], as well as a carrier of genes [12], enzymes and proteins [13]. HA is recognized as a promising biomaterial for bone due to its great biocompatibility potential [14–16] and its bioactivity and considering osteoinductivity [17], [18] and osteoconductivity [19], [20]. HA also plays a role in environmental remediation [21], as an advanced adsorbent material in the context of metal ion removal from wastewater [22], air pollution [23], soil [24], and water [25]. The use of HA proves to be very beneficial for removing contaminants present in the gaseous, liquid, and solid phases. HA is thermodynamically stable in crystalline form in body fluids and at room temperature and has a composition very similar to bone minerals [26].

The synthesis of hydroxyapatite in general can be done in two ways, namely synthesis from chemicals and extraction from biological resources [27]. Synthesis of chemicals using chemicals containing calcium (Ca) and phosphate $(PO_4)^{3-}$. Materials containing calcium include $Ca(NO_3)_2.4H_2O$, $Ca(NO_3)_2$ [28], $CaHPO_4$ [29] while phosphate-containing materials include H_3PO_4 [30], $NH_4H_2PO_4$ [31]. Extraction from biological resources includes shells, such as eggshells [30], shrimp shells [31], mammalian bones such as cows [32], camels [24], pig bones and dung [33], [34], horses, and aquatic animals such as fish bones [34] and scales [35], [36], shells [37], [38], sea corals, etc. In this study, the source of Ca and P used came from fish bones, because fish bones are waste that has not been utilized optimally and contains Ca and P at once [39-41], and the amount is abundant so that it can be processed into a more useful material, namely hydroxyapatite. HA has various forms with different characteristics, one of which is influenced by the synthesis method used and the preparation before the synthesis method is carried out. Synthesis methods that have been studied and developed include the sintering method [42], wet chemical method [43], mechanochemical method [44], sol-gel method [45], and hydrothermal method [46]. In addition to the synthesis method used the nature and character of HA are also influenced by the stages of sample preparation, including the sample munition process and the sample size to be processed further.

Preparation of bones to be used as samples needs to be done, considering that bones are natural materials found in animals and humans, of course, with the presence of bones mixed with other components that accompany bones in living things. The preparation phase aims to remove unwanted components such as dirt, fat, protein, and other components such as bone marrow and soft tissues [47-51]. Some literature explains that to remove organic components from bones it is easier to use boiling water [47], [48], combine bone washing with boiling water, and bone washing with organic solvents such as acetone or chloroform [49], [50], alternately wash bones using surfactant and alkaline solutions to remove soft tissue and remove cellulose [52]. Various methods of bone washing have been used with the same purpose, but produce different HA characters.

The next stage after bone preparation, namely the extraction of HA from fish bones using the calcination or sintering method which is a single process or a combination of calcination with other methods. The calcination process involves heating the bones in a furnace at different temperatures up to 1400 °C to remove organic matter completely and kill pathogens that may be present [53]. Based on this description, this study aims to determine the HA characteristics of acetone-soaked fish bones and disinterring in the form of fish bone powder using instruments Diffraction Sinar X. This study discusses the importance of the preparation stage before the sintering method is applied. Preparations can be ineffective if they use overly complicated procedures. A common method used at the preparation stage is soaking with acetone. The sample size referred to in this study is in the form of chunks (bulk) and powder (powder). The term refers to two different physical forms of material. They are distinguished by their structure and physical appearance, as well as how material particles are arranged or distributed in space.

EXPERIMENT

Material

Fish bones and acetone (p.a).

Instrument

X-ray diffraction D8 Advance Bruker AXS with LYNXEYE XE-T detector.

Procedure

Samples of raw fish bones were collected from the waste of a krupuk production house in Amplang, East Kalimantan. Fish bones are cleaned with running water to separate the head, body bones, and tail. In this study, the bones of the fish body were used. Fish bones are boiled with water for 1 hour to remove fat content (*defatting*), protein, and macroscopic impurities that stick, such as meat, bone marrow, and other attached soft tissues disappear entirely. Clean bone is soaked in acetone for 3 days where acetone is replaced every 24 hours with new acetone. Deproteinized products are stored in the oven at 80 °C to evaporate their water content [54]. The dried fish bones are crushed into small pieces using a mortar and pestle then ground into smaller particles using a blender and sifted 40 meshes to make the size uniform.

Compound Synthesis

A total of 20 g of bone is accurately weighed and fed into two alumina dishes and stored in a damping furnace for thermal processing. This process is carried out at a temperature of 900 °C for 4 hours with a heating rate of 5 °C / minute. The heated sample is slowly cooled to room temperature and stored for further analysis. Sample codes based on treatment are shown in **Table 1**.

Table 1. Sample code and treatment.

Sample Code	Acetone soaking	Drilling	Sieving	Sintering temperature (°C)	Sintering Time (hours)
FB	-	v	v	-	-
PAF-900	3 hari	v	v	900	4
CAF-900	3 hari	-	-	900	4
PWAF-900	-	v	v	900	4

Compound Characteristics

Sintered fish bone samples were characterized using instrumental techniques. Crystal properties and lattice parameters were determined by *D8 Advance Bruker AXS X-ray Diffraction analysis* with LYNXEYE XE-T *detector*. Data that has been obtained such as room group number, room group name, and grid parameters are inputted in the MATCH application. In addition, there are also data on the Miller index and FWHM (*Full Width at Half Maximum*) values and d_{hkl} values.

RESULTS AND DISCUSSION

Sintered fish bone samples were analyzed using X-ray Diffraction instruments, and then further analyzed. Based on the results of X-ray Diffraction data analysis, the similarity of compounds (compound formulas) HA matching results with JCPDS, percent crystallinity, lattice parameters, crystal field index (hkl), density and HA grain size can be obtained.

Based on the matching results between the sample diffractogram and JCPDS, the results shown in **Table 2** were obtained. Based on **Table 2**, it can be seen that the PAF-900 and CAF-900 samples are HA which has similarities with JCPDS 01-089-4405 with the compound formula $Ca_5(PO_4)_3OH$, while PWAF samples are HA which has similarities with JCPDS 01-075-3727 with compound formula $Ca_5(PO_4)_3(CO_3)_{0.01}(OH)_{1,3}$. This showed that samples of fish bone powder that were not soaked in acetone after the sintering process produced HA-containing carbonates. This indicates a variation in the composition of hydroxyapatite with a higher carbonate (CO_3^{2-}) content, as well as a slight change in the amount of hydroxyl (OH^-) in its structure. This may be due to the preparation process of PWAF-900 samples only by boiling to produce HA which still contains organic compounds such as carbonates.

Table 2. Results of matching compound formula and percent crystallinity HA.

JCPDS	01-075-3727	01-089-4405
Compound formula	$Ca_5(PO_4)_3(CO_3)_{0,01}(OH)_{1,3}$	$Ca_5(PO_4)_3OH$
	Crystallinity (%)	Crystallinity (%)
FB		50,933
PAF-900		84,767
CAF-900		73,506
PWAF-900	71,962	

Fish bones contain a variety of organic and inorganic compounds. If fish bones are not subjected to soaking with acetone before the sintering process, carbonate groups may remain in their structure. This happens because fish bones

contain the minerals calcium phosphate and calcium carbonate. When fish bones are soaked in acetone before the sintering process, acetone serves to remove most of the organic compounds, including fats and proteins, present in the bones. During the sintering process, which is a high-heating process to make solid material from solid powder or chunks, the carbonate groups remaining in the fishbone can undergo decomposition. The decomposition reaction of calcium carbonate ($CaCO_3$) can be expressed as follows:

$$CaCO_{3(s)} \rightarrow CaO_{(s)} + CO_{2(g)}$$

Based on the reaction, calcium carbonate decomposes into calcium oxide (burnt lime) and carbon dioxide. Carbon dioxide will be released in gaseous form, while calcium oxide will remain in the sample. PWAF-900 samples still contain carbonate after the sintering process, this is possible that substitution has occurred. Usually, carbonate ions replace phosphate ions in their structure, so their characteristic parameters change depending on the composition of the carbonate content, and the presence of carbonate will change its chemical properties. Based on this, the preparation stage affects the resulting HA structure.

Table 2 also shows that the sintering process can increase the percent crystallinity of fish bone samples. FB samples with a crystallinity percent of 50,933% after being sintered at 900 °C for 4 hours increased the percent crystallinity to 84,767% in PAF-900 and 73,506% in CAF-900 and 71,962% in PWAF-900. This is because heat causes particles to coalesce and the effectiveness of surface tension reactions increases, in other words, the sintering process causes particles to unite in such a way that their density increases [55]. During this process, grain boundaries are formed, which is the initial stage of recrystallization. Higher sintering temperatures can increase the rate of diffusion of atoms and molecules in the material. This can help shrinkage and the formation of a more regular crystal structure, thereby increasing the percentage of HA crystallization.

Based on **Table 2** it can be seen that PAF-900 samples have a higher crystallization percent than CAF-900 samples, this is because the crystal structure of PAF-900 is easier to form because it is powdered and well arranged at larger grain sizes, so the percent crystallinity can be higher in finer powders. In addition, PAF-900 samples tend to have a smaller, finer, and uniform particle size distribution than chunk-shaped CAF-900 samples. Smaller particles have a larger surface area and tend to be more susceptible to crystal growth during the sintering process. PAF-900 samples can produce a higher percent crystallinity than CAF-900 samples because the particle size is smaller and the particle distribution is more uniform.

The percent crystallization of PAF-900 samples is higher than PWAF-900 samples, this is likely because PWAF-900 samples still have impurities or organic compounds. Controlling impurities in sample preparation can also affect the HA crystallization process. Some elements or compounds can act as catalysts or inhibitors in crystallization reactions. The addition of carbonate, phosphate, and hydroxyl groups compared to ordinary HA compounds in PWAF-900 samples will affect the stability of the crystal structure and the crystallinity of HA.

The results of X-ray Diffraction analysis can also be used to determine the parameters of the HA crystal lattice in all four samples (**Table 3**).

Table 3 . Material grating parameters

Sample	Shape	a (Å)	b (Å)	c (Å)	I/I_0	Density (g/cm^3)
FB	hexagonal	9,4210	9,4210	6,8800	1,10	2.812
PAF-900	hexagonal	9,4212	9,4212	6,8 927	1, 03	3.149
CAF-900	hexagonal	9, 4394	9, 4394	6, 8861	1, 03	3.149
PWAF-900	hexagonal	9,4 394	9,4 394	6, 8861	1, 03	3,1 46

The HA structure obtained by the crystal system is hexagonal with cell parameter values a = b ≠ c and a *space group P 63 / m*, where the entire sample has a price range *of a = b = 9,42 Å and c = 6,88 Å.* HA density increases after sintering. The sintering process involves applying pressure and heat to a material without melting it to unite particles into a solid mass. The fusion between particles is also called *interparticle necking* which plays an important role in producing products with high density [55]. The sintering process with higher temperatures causes HA particles to tend to shrink and denser each other. This process can reduce porosity and increase adhesion between particles, which in turn can increase crystal density. An increase in sintering temperature can trigger more active chemical reactions between components in the sample, aiding the formation of a larger, denser

crystalline phase. It can also reduce the number of amorphous or irregular phases, which can lead to higher crystal densities. Higher sintering temperatures can increase the rate of atomic diffusion and molecular migration in the material. This can help HA particles "move" closer to each other and form a more orderly and dense crystal structure.

The results of X-ray diffraction analysis can also be used to determine the HA crystal field index of all four samples (**Table 4**).

Table 4. Diffraction result of crystal plane index [hkl] HA.

2θ	25,8	31,7	32,1	32,8	34,0	39,7	46,6	57,4	50,4
Reference	[56]–[58]	[56]–[58]	[58], [59]	[58], [59]	[58], [59]	[57], [59]	[57], [59]	[58], [59]	[57], [59]
FB	25,80	31,91	-	-	-	-	46,64	49,61	-
PAF-900	25,90	31,72	32,15	32,86	34,02	39,74	46,67	49,45	50,43
CAF-900	25,83	31,70	32,10	32,82	33,95	39,72	46,63	-	-
PWAF-900	25,79	31,60	32,09	32,71	33,97	39,61	46,54	49,35	50,31
hkl	002	211	112	300	202	310	222	213	321
d (Z)	3,45	2,82	2,78	2,72	2,63	2,26	1,94	1,84	1,81

Based on **Table 4**, it can be seen that PAF-900, CAF-900, and PWAF-900 samples predominantly contain HA. The crystallinity of HA is identified through a typical peak at XRD at 2θ = 25,8 (002); 31,7 (211); 32,1 (112); 32,8 (300); 34,0 (202); 39,7 (310); 46,6 (222); 49,4 (213); 50.4 (321) [57], [59-61]. The peaks are shown in **Figure 1** and **Figure 2**.

From the XRD data of HA compounds obtained, it can be calculated the HA particle size using the Scherrer equation [62]. The similarities are

$$D = \frac{K \cdot \lambda}{\beta . cos cos \theta} \quad (1)$$

where D = crystal size (nm), K = crystal form factor, λ = X-ray wavelength (0.15406), β = FWHM value (rad), θ = diffraction angle. The average particle size is obtained from the average value of the particle size at each diffraction angle in each sample. A quick look at the calculations for determining the average particle size of a sample using the Scherrer equation is presented in **Table 5**.

Table 5. The result of calculating the crystal size at the diffraction peak HA.

Sample	2θ (°)	K	λ (nm)	FWHM (radian)	Grain size (nm)	Average grain size (nm)
FB	31,91	0,9	0,1541874	1,9553	0,073813992	0,0905
	25,8	0,9	0,1541874	0,9914	0,14359663	
	49,61	0,9	0,1541874	2.8164	0,054279416	
PAF-900	31,72	0,9	0,1541874	0,1792	0.80502407	0,8964
	32,86	0,9	0,1541874	0,1725	0.838703616	
	32,15	0,9	0,1541874	485.29	0,000297586	
CAF-900	31,7	0,9	0,1541874	0,2102	0,686266235	0,6808
	32,82	0,9	0,1541874	0,2484	0,582373156	
	32,1	0,9	0,1541874	0,1866	0,773832511	
PWAF-900	31,6	0,9	0,1541874	0,2112	0,682847945	0,7398
	32,71	0,9	0,1541874	0,2274	0,635974817	
	32,09	0,9	0,1541874	0,1603	0,900770568	

Based on the Scherrer equation, it can be seen that the average particle size in the PAF-900 sample was obtained at 0,8964 nm, while in the CAF-900 and PWAF-900 samples, it was 0,6808 and 0,7398 nm respectively. The larger the FWHM, the smaller the grain size, as summarized in **Table 5**. This is because the larger the size of the crystal grain, the X-ray diffraction peaks produced will be sharper and narrower, resulting in a smaller FWHM. Conversely, the smaller the crystal grain size, the resulting diffraction peak will be wider, resulting in a larger FWHM. It can be seen that FB samples have a grain size of 0,0905 nm, after undergoing sintering at a temperature of 900 °C for 4 hours, the grain size increases as found in PAF-900, CAF-900, and PWAF-900 samples.

The effect of sintering on grain size depends on the process of necking formation. The formation of *necking* occurs as a result of sintering and diffusion driven by the desire of particles to minimize energy [63]. For the sintering process, there are three important stages, namely the initial stage, the intermediate stage, and the final stage. At the initial stage, grain boundaries begin to form

between each particle in contact with each other through diffusion, which is called "necking". As Dai et al. have already mentioned, in 2019 [64], the fastest *necking radius* seems to occur in the early stages. The shape of the neck is affected by the energy difference arising from the particles and the double curvature of the neck. During the initial phase of neck formation, diffusion on the surface is usually the dominant mass transfer mechanism when powdered. The compacted ones are heated to sintering temperature [65], [66]. This stage is also known as the "neck growth" stage. The next stage is the intermediate stage where when sintering occurs, adjacent necks tend to collide with each other. At this stage also occurs compaction and growth of grains. The density of the material is very important because, in the final stage, it will result in fewer pores. Another factor is the formation of new contact points within the pore itself through pore shrinkage [67]. Therefore, it shows that the most important stage in sintering is pore shrinkage. At this stage, pore shrinkage can occur either due to expansion where solid particles enter the pore or gases that are inside the pore are released into the environment [68]. To minimize surface energy, atoms near the boundary of each particle migrate together and form a neck. Due to the deformation of particles in response to sintering stress, the flow of plastic through dislocation movements can promote neck growth and compaction.

The grain size of the PAF-900 sample is larger than that of PWAF-900, this may be due to the presence of other phases in the PWAF-900 sample, thus inhibiting grain growth. The interaction between various components in PWAF-900 can affect grain growth and produce different grain sizes. The grain size in the PAF-900 sample is larger than that of CAF-900, this is due to surface reactivity, where the surface of fish bone powder may be more reactive than the surface of the fishbone lump, allowing for fusion and growth of more grains during sintering. PAF-900 samples have a larger initial surface area than CAF-900 samples, so during the sintering process, powder particles have more contact points and possible fusion between particles, which can lead to greater grain growth. PAF-900 samples tend to be more homogeneous in composition and particle size than CAF-900 samples, which in turn can result in a more even heat distribution during sintering, resulting in greater grain growth. Careful characterization and understanding of the interactions between these factors are necessary to understand and control the final grain size of HA during the sintering process.

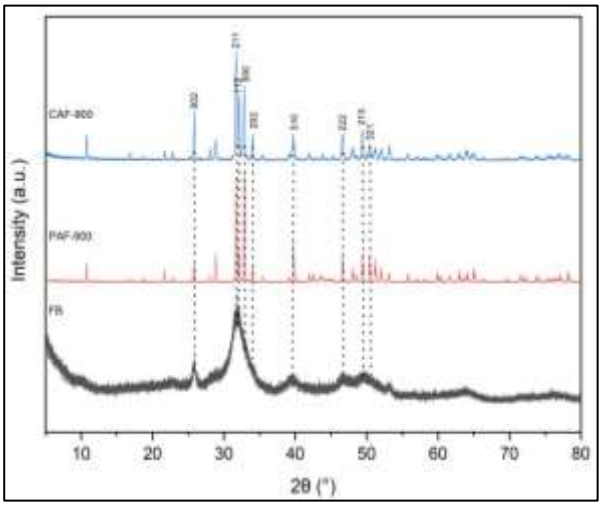

Figure 1 . Peak comparison of FB, PAF-900, and CAF-900 samples.

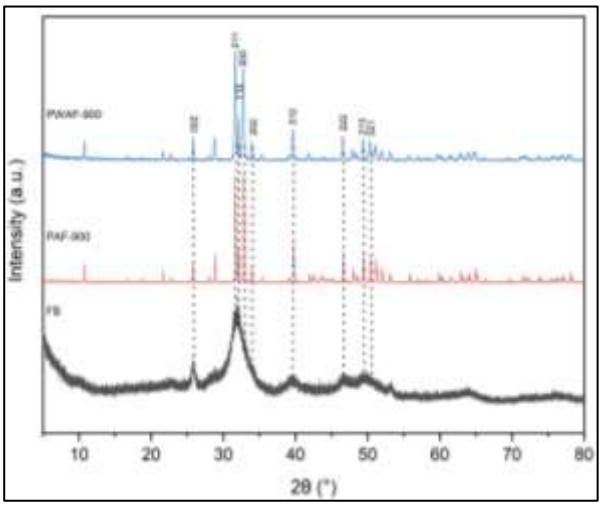

Figure 2. Peak comparison on FB, PAF-900, and PWAF-900 samples.

Based on **Figure 1** and **Figure 2** it can be seen that the FB sample has an XRD pattern that does not show sharp peaks that are usually associated with crystal structure. This shows that FB has amorphous or semicrystalline properties so it is detected to have a lower percent crystallinity than other samples. FB's structure means it is more random and doesn't have a regular crystal circuit. This may indicate the presence of an amorphous structure or the possible presence of a noncrystalline phase. The XRD pattern exhibits amorphous properties, not absolute information that raw bone contains no crystalline material at all. There is a crystalline phase with a smaller proportion or on a larger scale smaller by 50,933% as written in **Table 1**.

Based on **Figure 1** It can be seen that the base peak in the PAF-900 sample band is narrower, higher, and more numerous than the CAF-900

sample, this indicates that in the PAF-900 sample, there are more crystals and have a larger crystal size, so the X-ray interaction with the crystal structure in the sample is more. This corresponds to the percent crystallinity of PAF-900 samples which is more than the percent crystallinity of CAF-900 as shown in Table 1 and Table 4. Based on **Figure 2** It can be seen that the peak in the PAF-900 sample band is higher than in the PWAF-900 sample, this is because the PAF-900 sample has larger and uniform crystals, so X-ray interactions with crystal structure in the sample are more.

CONCLUSION

The preparation stage of fish bones by acetone immersion and sample size affect the resulting HA character including compound formula, percent crystallinity, density, and HA grain size. HA produced from the extraction of acetone-soaked fish bones is higher in percent crystallinity, longer grain size, and denser density than HA obtained from fish bones without acetone-soaked. The resulting HA powder has a higher percent crystallinity, longer grain size, and denser density than HA chunks.

ACKNOWLEDGEMENT

The author would like to thank the research grant for the TA Doctoral Dissertation Research Grant of the Ministry of Education and Culture and Technology 2023 with contract number: 3018/UN6.3.1/PT.00/2023.

REFERENCE

[1] Y. Cai, H. Li, M. Karlsson, K. Leifer, H. Engqvist, and W. Xia, “Biomineralization on single crystalline rutile: the modulated growth of hydroxyapatite by fibronectin in a simulated body fluid”, *RSC Adv.*, **6**(42), 35507–35516, 2016, doi: 10.1039/C6RA04303H.

[2] J. Guan *et al.*, “Bioinspired nanostructured hydroxyapatite/collagen three-dimensional porous scaffolds for bone tissue engineering”, *RSC Adv.*, **5**(46), 36175–36184, 2015, doi: 10.1039/C5RA01487E.

[3] L. Morejón *et al.*, “Development, characterization and in vitro biological properties of scaffolds fabricated from calcium phosphate nanoparticles”, *Int. J. Mol. Sci.*, **20**(7), 2019, doi: 10.3390/ijms20071790.

[4] S. Kojima, H. Nakamura, S. Lee, F. Nagata, and K. Kato, “Hydroxyapatite formation on self-assembling peptides with differing secondary structures and their selective adsorption for proteins”, *Int. J. Mol. Sci.*, **20**(18), 2019, doi: 10.3390/ijms20184650.

[5] Y.-Y. Hu, A. Rawal, and K. Schmidt-Rohr, “Strongly bound citrate stabilizes the apatite nanocrystals in bone”, *Proc. Natl. Acad. Sci.*, **107**(52), 22425–22429, Dec. 2010, doi: 10.1073/pnas.1009219107.

[6] M.T. Islam, R.M. Felfel, E.A. Abou Neel, D.M. Grant, I. Ahmed, and K.M.Z. Hossain, “Bioactive calcium phosphate–based glasses and ceramics and their biomedical applications: A review”, *J. Tissue Eng.*, **8**, 2041731417719170, 2017, doi: 10.1177/2041731417719170.

[7] Y. Bala and E. Seeman, “Bone’s material constituents and their contribution to bone strength in health, disease, and treatment”, *Calcif. Tissue Int.*, **97**(3), 308–326, 2015, doi: 10.1007/s00223-015-9971-y.

[8] K. Bechara *et al.*, "A histological study of non-ceramic hydroxyapatite as a bone graft substitute material in the vertical bone augmentation of the posterior mandible using an interposition inlay technique: A split-mouth evaluation", *Ann. Anat. - Anat. Anz.*, **202**, 1–7, 2015, doi: 10.1016/j.aanat.2015.07.004.

[9] A.H. Dewi and I.D. Ana, “The use of hydroxyapatite bone substitute grafting for alveolar ridge preservation, sinus augmentation, and periodontal bone defect: A systematic review”, *Heliyon*, **4**(10), e00884, 2018, doi: 10.1016/j.heliyon.2018.e00884.

[10] J. Ran *et al.*, “Constructing multi-component organic/inorganic composite bacterial cellulose-gelatin/hydroxyapatite double-network scaffold platform for stem cell-mediated bone tissue engineering”, *Mater. Sci. Eng. C*, **78**, 130–140, 2017, doi: 10.1016/j.msec.2017.04.062.

[11] M.C. Lee *et al.*, "Development of novel gene carrier using modified nano-hydroxyapatite derived from equine bone for osteogenic differentiation of dental pulp stem cells", *Bioact. Mater.*, **6**(9), 2742–2751, 2021, doi: 10.1016/j.bioactmat.2021.01.020.

[12] J. Huang, S. Sebastian, M. Collin, M. Tägil, L. Lidgren, and D.B. Raina, "A calcium sulfate/hydroxyapatite ceramic biomaterial carrier for local delivery of tobramycin in bone infections: Analysis of rheology, drug

release, and antimicrobial efficacy", *Ceram. Int.*, 2023, doi: 10.1016/j.ceramint.2023.08.064.

[13] Y.Q. Almulaiky *et al.*, "Hydroxyapatite-decorated ZrO_2 for α-amylase immobilization: Toward the enhancement of enzyme stability and reusability", *Int. J. Biol. Macromol.*, **167**, 299–308, 2021, doi: 10.1016/j.ijbiomac.2020.11.150.

[14] J. Fang, P. Li, X. Lu, L. Fang, X. Lü, and F. Ren, "A strong, tough, and osteoconductive hydroxyapatite mineralized polyacrylamide/dextran hydrogel for bone tissue regeneration", *Acta Biomater.*, **88**, 503–513, 2019, doi: 10.1016/j.actbio.2019.02.019.

[15] C. Li, W. Qin, S. Lakshmanan, X. Ma, X. Sun, and B. Xu, "Hydroxyapatite based biocomposite scaffold: A highly biocompatible material for bone regeneration", *Saudi J. Biol. Sci.*, **27**(8), 2143–2148, 2020, doi: 10.1016/j.sjbs.2020.05.029.

[16] M.N. Salimi and A. Anuar, "Characterizations of Biocompatible and Bioactive Hydroxyapatite Particles", *Malays. Tech. Univ. Conf. Eng. Amp Technol. 2012 MUCET 2012*, **53**, 192–196, 2013, doi: 10.1016/j.proeng.2013.02.025.

[17] L. Cheng *et al.*, "Osteoinduction of hydroxyapatite/β-tricalcium phosphate bioceramics in mice with a fractured fibula" *Acta Biomater.*, **6**(4), 1569–1574, 2010, doi: 10.1016/j.actbio.2009.10.050.

[18] X. Wei, X. Zhang, Z. Yang, L. Li, and H. Sui, "Osteoinductive potential and antibacterial characteristics of collagen-coated iron oxide nanosphere containing strontium and hydroxyapatite in long term bone fractures", *Arab. J. Chem.*, **14**(3), 102984, 2021.

[19] B.-S. Chang *et al.*, "Osteoconduction at porous hydroxyapatite with various pore configurations", *Biomaterials*, **21**(12), 1291–1298, 2000, doi: 10.1016/S0142-9612(00)00030-2.

[20] Q. Wang *et al.*, "Experimental and simulation studies of strontium/zinc-codoped hydroxyapatite porous scaffolds with excellent osteoinductivity and antibacterial activity", *Appl. Surf. Sci.*, **462**, 118–126, 2018, doi: 10.1016/j.apsusc.2018.08.068.

[21] N.A.S. Mohd Pu'ad, P. Koshy, H.Z. Abdullah, M.I. Idris, and T.C. Lee, "Syntheses of hydroxyapatite from natural sources", *Heliyon*, **5**(5), e01588, 2019, doi: 10.1016/j.heliyon.2019.e01588.

[22] H. Wu, H. Yan, Y. Quan, H. Zhao, N. Jiang, and C. Yin, "Recent progress and perspectives in bio trickling filters for VOCs and odorous gases treatment", *J. Environ. Manage.*, **222**, 409–419, 2018, doi: 10.1016/j.jenvman.2018.06.001.

[23] M. Bin Mobarak *et al.*, "Environmental remediation by hydroxyapatite: Solid state synthesis utilizing waste chicken eggshell and adsorption experiment with Congo red dye" *J. Saudi Chem. Soc.*, **27**(5), 101690, Sep. 2023, doi: 10.1016/j.jscs.2023.101690.

[24] R.A. Alsaiari, E.M. Musa, and M.A. Rizk, "Biodiesel production from date seed oil using hydroxyapatite-derived catalyst from waste camel bone", *Heliyon*, **9**(5), e15606, 2023, doi: 10.1016/j.heliyon.2023.e15606.

[25] C.R. Holkar, A.J. Jadhav, D.V. Pinjari, N.M. Mahamuni, and A.B. Pandit, "A critical review on textile wastewater treatments: Possible approaches", *J. Environ. Manage.*, **182**, 351–366, 2016, doi: 10.1016/j.jenvman.2016.07.090.

[26] M. Sadat-Shojai, M.-T. Khorasani, E. Dinpanah-Khoshdargi, and A. Jamshidi, "Synthesis methods for nanosized hydroxyapatite with diverse structures", *Acta Biomater.*, **9**(8), 7591–7621, 2013, doi: 10.1016/j.actbio.2013.04.012.

[27] N.A.S. Mohd Pu'ad, P. Koshy, H.Z. Abdullah, M.I. Idris, and T.C. Lee, "Syntheses of hydroxyapatite from natural sources", *Heliyon*, **5**(5), e01588, 2019, doi: 10.1016/j.heliyon.2019.e01588.

[28] C.R. Akshata, G. Harichandran, and E. Murugan, "Effect of pectin on the crystallization of strontium substituted HA for bone reconstruction application", *Colloids Surf. B Biointerfaces*, **226**, 113312, 2023, doi: 10.1016/j.colsurfb.2023.113312.

[29] C. Li-yun, Z. Chuan-bo, and H. Jian-feng, "Influence of temperature, $[Ca^{2+}]$, Ca/P ratio and ultrasonic power on the crystallinity and morphology of hydroxyapatite nanoparticles prepared with a novel ultrasonic precipitation method", *Mater. Lett.*, **59**(14), 1902–1906, 2005, doi: 10.1016/j.matlet.2005.02.007.

[30] X. Zhao *et al.*, "Preparation of carbon fiber/Mg-doped nano-hydroxyapatite composites under low temperature by pressureless sintering", *Ceram. Int.*, **48**(1), 674–683, 2022, doi: 10.1016/j.ceramint.2021.09.147.

[31] M. Baladi *et al.*, "Green sol–gel synthesis of hydroxyapatite nanoparticles using lemon extract as capping agent and investigation of its anticancer activity against human cancer cell lines (T98, and SHSY5)", *Arab. J. Chem.*, **16**(4), 104646, 2023, doi: 10.1016/j.arabjc.2023.104646.

[32] A.R. Noviyanti, I. Rahayu, R.P. Fauzia, and Risdiana, "The effect of Mg concentration to the mechanical strength of hydroxyapatite derived from eggshell", *Arab. J. Chem.*, **14**(4), 103032, 2021, doi: 10.1016/j.arabjc.2021.103032.

[33] T.S. Trung *et al.*, "Valorization of fish and shrimp wastes to nano-hydroxyapatite/chitosan biocomposite for wastewater treatment", *J. Sci. Adv. Mater. Devices*, **7**(4), 100485, 2022, doi: 10.1016/j.jsamd.2022.100485.

[34] M. Nurhadi, R. Kusumawardani, W. Wirhanuddin, R. Gunawan, and H. Nur, "Carbon-containing hydroxyapatite obtained from fish bone as low-cost mesoporous material for methylene blue adsorption", *Bull. Chem. React. Eng. Catal.*, **14**(3), 660–671, 2019, doi: 10.9767/bcrec.14.3.5365.660-671.

[35] A.M. Castillo-Paz, M. Gomez-Resendiz, D.F. Cañon-Davila, B.A. Correa-Piña, R. Ramírez-Bon, and M.E. Rodriguez-Garcia, "The effect of temperature on the physical-chemical properties of bovine hydroxyapatite biomimetic scaffolds for bone tissue engineering", *Ceram. Int.*, 2023, doi: 10.1016/j.ceramint.2023.08.065.

[36] E.A. Ofudje, A. Rajendran, A.I. Adeogun, M.A. Idowu, S.O. Kareem, and D.K. Pattanayak, "Synthesis of organic derived hydroxyapatite scaffold from pig bone waste for tissue engineering applications", *Adv. Powder Technol.*, **29**(1), 1–8, 2018, doi: 10.1016/j.apt.2017.09.008.

[37] J. Liao, X. He, Y. Zhang, L. Zhang, and Z. He, "The construction of magnetic hydroxyapatite-functionalized pig manure-derived biochar for the efficient uranium separation", *Chem. Eng. J.*, **457**, 141367, Feb. 2023, doi: 10.1016/j.cej.2023.141367.

[38] V. Boursiaki *et al.*, "Skeletal deformity of scoliosis in gilthead seabreams (sparus aurata): association with changes to calcium-phosphor hydroxyapatite salts and collagen fibers", *Water*, **11**(2), 2019, doi: 10.3390/w11020257.

[39] P.V. Nam, N.V. Hoa, and T.S. Trung, "Properties of hydroxyapatites prepared from different fish bones: A comparative study", *Ceram. Int.*, **45**(16), 20141–20147, 2019, doi: 10.1016/j.ceramint.2019.06.280.

[40] S. Meski *et al.*, "Synthesis of hydroxyapatite from mussel shells for effective adsorption of aqueous Cd(II)", *Water Sci. Technol. J. Int. Assoc. Water Pollut. Res.*, **80**(7), 1226–1237, Oct. 2019, doi: 10.2166/wst.2019.366.

[41] R. Ismail *et al.*, "Characterization of PLA/PCL/Green mussel shells hydroxyapatite (HA) biocomposites prepared by chemical blending methods", *Materials*, **15**(23), 2022, doi: 10.3390/ma15238641.

[42] I. Kusumaningrum and A.N. Asikin, "Karakteristik kerupuk ikan fortifikasi kalsium dari tulang ikan belida", *J. Pengolah. Has. Perikan. Indones.*, **19** (3), 233–240.

[43] H.F. Putranto, A.N. Asikin, and I. Kusumaningrum, "Karakterisasi tepung tulang ikan belida (Chitala SP.) sebagai sumber kalsium dengan metode hidrolisis protein", *Ziraaah Maj. Ilm. Pertan.*, **41**(1), 11–20, 2016, doi: 10.31602/zmip.v41i1.315.

[44] E. Mahmuda, N. Idiawati, and M.A. Wibowo, "Ekstraksi gelatin pada tulang ikan belida (Chitala lopis) dengan proses perlakuan asam klorida", *J. Kim. Khatulistiwa*, **7** (4), 114–123, 2018.

[45] P.R. Minim *et al.*, "The combined effects of binder addition and different sintering methods on the mechanical properties of bovine hydroxyapatite", *J. Mech. Behav. Biomed. Mater.*, **144**, 105993, 2023, doi: 10.1016/j.jmbbm.2023.105993.

[46] E.S. Krishna and G. Suresh, "Development and characterization of acicular nano-hydroxyapatite powder from wet chemical synthesis method", *Int. Conf. Mater. Mech. Model.*, **56**, 781–784, 2022, doi: 10.1016/j.matpr.2022.02.256.

[47] B.M. Ferrairo *et al.*, "Production of bovine hydroxyapatite nanoparticles as a promising biomaterial via mechanochemical and sonochemical methods", *Mater. Chem. Phys.*, **295**, 127046, 2023, doi: 10.1016/j.matchemphys.2022.127046.

[48] H. Chen, R. Wang, L. Qian, H. Liu, J. Wang, and M. Zhu, "Surface modification of urchin-like serried hydroxyapatite with sol-gel method and its application in dental composites", *Compos. Part B Eng.*, **182**, 107621, 2020, doi: 10.1016/j.compositesb.2019.107621.

[49] L.F. Zubieta-Otero and M.E. Rodriguez-Garcia, "Obtention and characterization of nano bio-hydroxyapatite particles by combined hydrothermal alkaline and ultrasonic wet milling methods", *Mater.*, **1**(3), 100019, 2023, doi: 10.1016/j.nxmate.2023.100019.

[50] M.R. Ayatollahi, M.Y. Yahya, H. Asgharzadeh Shirazi, and S.A. Hassan, "Mechanical and tribological properties of hydroxyapatite nanoparticles extracted from natural bovine bone and the bone cement developed by nano-sized bovine hydroxyapatite filler", *Ceram. Int.*, **41**(9), Part A, 10818–10827, 2015, doi: 10.1016/j.ceramint.2015.05.021.

[51] E. Hosseinzadeh, M. Davarpanah, N.H. Nemati, and S. Tavakoli, "Fabrication of a hard tissue replacement using natural hydroxyapatite derived from bovine bones by thermal decomposition method", *Int. J. Organ Transplant. Med.*, **5**(1), 23, 2014.

[52] N.A.M. Barakat, M.S. Khil, A.M. Omran, F.A. Sheikh, and H.Y. Kim, "Extraction of pure natural hydroxyapatite from the bovine bones bio waste by three different methods", *J. Mater. Process. Technol.*, **209**(7), 3408–3415, 2009, doi: 10.1016/j.jmatprotec.2008.07.040.

[53] M. Akram, R. Ahmed, I. Shakir, W.A.W. Ibrahim, and R. Hussain, "Extracting hydroxyapatite and its precursors from natural resources", *J. Mater. Sci.*, **49**(4), 1461–1475, 2014, doi: 10.1007/s10853-013-7864-x.

[54] R. Murugan, S. Ramakrishna, and K.P. Rao, "Nanoporous hydroxy-carbonate apatite scaffold made of natural bone", *Mater. Lett.*, **60**(23), 2844–2847, 2006, doi: 10.1016/j.matlet.2006.01.104.

[55] M.R. Mazlan *et al.*, "Necking mechanism under various sintering process parameters – A review", *J. Mater. Res. Technol.*, **23**, 2189–2201, 2023, doi: 10.1016/j.jmrt.2023.01.013.

[56] J. Venkatesan, Z.J. Qian, B. Ryu, N.V. Thomas, and S.K. Kim, "A comparative study of thermal calcination and an alkaline hydrolysis method in the isolation of hydroxyapatite from Thunnus obesus bone", *Biomed. Mater.*, **6**(3), 035003, Apr. 2011, doi: 10.1088/1748-6041/6/3/035003.

[57] A. Mathirat *et al.*, "Remineralizing potential of natural nano-hydroxyapatite obtained from epinephelus chlorostigma in artificially induced early enamel lesion: An in vitro study.," *Nanomater. Basel Switz.*, **12**(22), 2022, doi: 10.3390/nano12223993.

[58] P. Shi, M. Liu, F. Fan, C. Yu, W. Lu, and M. Du, "Characterization of natural hydroxyapatite originated from fish bone and its biocompatibility with osteoblasts", *Mater. Sci. Eng. C*, **90**, 706–712, 2018, doi: 10.1016/j.msec.2018.04.026.

[59] J. Venkatesan, S.-K. Kim, and S. Kim, *Hydroxyapatite from marine fish bone: isolation and characterization techniques*. CRC Press Boca Raton, USA, 2016.

[60] B.-H. Chen, K.-I. Chen, M.-L. Ho, H.-N. Chen, W.-C. Chen, and C.-K. Wang, "Synthesis of calcium phosphates and porous hydroxyapatite beads prepared by emulsion method", *Mater. Chem. Phys.*, **113**(1), 365–371, 2009, doi: 10.1016/j.matchemphys.2008.06.040.

[61] P. Shi, M. Liu, F. Fan, C. Yu, W. Lu, and M. Du, "Characterization of natural hydroxyapatite originated from fish bone and its biocompatibility with osteoblasts", *Mater. Sci. Eng. C*, **90**, 706–712, 2018, doi: 10.1016/j.msec.2018.04.026.

[62] M. Sumadiyasa and I.B.S. Manuaba, "Penentuan ukuran kristal menggunakan formula scherrer, williamson-hull plot dan ukuran partikel dengan SEM", *Bul Fis FMIPA UNUD Bul.*, **19**(1), 28–35, 2018.

[63] J.G. Miranda-Hernández, H. Herrera-Hernández, C.O. González-Morán, J.N. Rivera Olvera, I. Estrada-Guel, and F. Botello Villa, "Synthesis and characterization of Zn-Nix advanced alloys prepared by mechanical milling and sintering at solid-state process", *Adv. Mater. Sci. Eng.*, **2017**, 7967848, 2017, doi: 10.1155/2017/7967848.

[64] H. Dai, D. Chen, and Z. Zheng, "Modelling the sintering neck growth process of metal fibers under the surface diffusion mechanism using the lattice Boltzmann method", *Metals*, **9**(5), 614, 2019.

[65] K. Nishiyabu, "15 - Powder space holder metal injection molding (PSH-MIM) of micro-porous metals," in *Handbook of Metal Injection Molding*, D.F. Heaney, Ed., Woodhead Publishing, 2012, 349–390. doi: 10.1533/9780857096234.3.349.

[66] H.N. Yoshimura, A.L. Molisani, N.E. Narita, P.F. Cesar, and H. Goldenstein, "Porosity dependence of elastic constants in aluminum nitride ceramics", *Mater. Res.*, **10**, 127–133, 2007.

[67] F.F. Lange, "Densification of powder compacts: An unfinished story", *Dev. Ceram. Sci. Eng. Last 50 Years Meet. Celebr. Profr. Sir Richard Brooks 70th Birthd.*, **28**(7), 1509–1516, 2008, doi: 10.1016/j.jeurceramsoc.2007.12.016.

[68] M.N. Rahaman, "Series materials engineering," (Marcel Dekker, Inc.): 10., New York : M. Dekker, c1995.